Analytical and experimental characterization of metasurfaces with normal polarizability

Davor Zaluški, Anthony Grbic, and Silvio Hrabar

Phys. Rev. B **93**, 155156 — Published 27 April 2016

DOI: 10.1103/PhysRevB.93.155156

Analytical and Experimental Characterization of Metasurface With Normal Polarizability

Davor Zaluški[1], Anthony Grbic[2], Silvio Hrabar[1]
[1]University of Zagreb, Faculty of Electrical Engineering and Computing,
Department of Wireless Communications, Unska 3, Zagreb, Croatia
[2]Department of Electrical Engineering and Computer Science,
University of Michigan, Ann Arbor, MI, 48109-2122, USA
Davor.Zaluski@fer.hr, agrbic@umich.edu, Silvio.Hrabar@fer.hr

To date, research on metasurfaces has predominantly focused on those with polarizabilities that are tangent to the metasurface. A few theoretical works have characterized metasurfaces with normal polarizabilities. In fact, experimental extraction of the surface polarizabilities of such metasurfaces has not been reported to date. Here, we provide full analytical, numerical, and experimental characterizations of a metasurface that can be described with polarizabilities in all three spatial directions. First, a set of equations is derived that allows a surface distribution of scatterers to be replaced by a sheet boundary condition. It is shown that the extraction of unknown polarizabilities in the normal direction necessarily requires scattering parameters obtained from oblique incidence. Closed-form expressions that relate scattering parameters to surface susceptibilities in all three spatial directions are given. It is shown that the reflection and transmission properties of the metasurface can be predicted, for an arbitrary angle of incidence, from the sheet parameters. In addition, we report the experimental characterization of a metasurface with polarizabilities in the normal direction. The free-space measurements were performed on a recently proposed DB surface at 10 GHz. Experiments confirmed that the sheet parameters do not change with angle of incidence. Consequently, it was possible to extract surface susceptibilities in the normal direction from measured transmission parameters alone.

PACS numbers: 81.05.Xj, 41.20.Jb

1. INTRODUCTION

Metamaterials are artificial structures engineered to have tailored electromagnetic properties, usually not found in natural homogenous materials. Early research efforts in metamaterials were based on exploring novel physical phenomena such as backward propagation and a negative index of refraction, subwavelength guiding of electromagnetic energy, subwavelength lensing [1], and their engineering realization [2 – 6]. Metamaterials consist of subwavelength scatterers arranged in a regular or irregular lattice of subwavelength spacing to obtain desired bulk electromagnetic properties [7, 8]. As a result, they can be homogenized and modeled using effective-medium theory. The homogenization process averages the electric and magnetic fields over a unit cell of the metamaterial in order to calculate effective material parameters: permittivity and permeability [9 – 11]. Despite the efforts put into the field of metamaterials over the past decade, there are few practical real-world engineering applications for these bulk materials. The basic reasons lie in the significant losses associated with the inherent resonant nature of metamaterials, and complex fabrication.

Recently, there has been increased interest in metasurfaces [12, 13]. A metasurface is a periodic structure composed of electrically small scatterers arranged in a two-dimensional pattern, the thickness and periodicity of which are much smaller than the wavelength in the surrounding medium. In other words, a metasurface is the two-dimensional equivalent of a bulk 3D metamaterial. Compared to metamaterials, metasurfaces take up less physical space, and offer reduced losses. In addition, metasurfaces allow practical tunability / controllability mechanisms, novel wave-guiding structures and boundary conditions [14 – 16].

Attempts to use effective bulk parameters to characterize metasurfaces proved to be inappropriate [17, 18]. In order to characterize a metasurface with effective parameters (effective permittivity and effective permeability), one needs to introduce a thickness. However, the thickness of a metasurface is ill-defined, leading to an ambiguity in material parameters. For instance, authors have found that one cannot define bulk parameters (ε and μ) that are independent of structure thickness [17, 18].

Instead, a metasurface can be characterized in terms of the electric and magnetic polarizabilities of the scatterers that compose it. In [19], it was shown that these surface polarizabilities are unique properties of a metasurface, and therefore best suited for their characterization. Most earlier attempts to characterize a metasurface were focused on metasurfaces with scatterers that can be described with polarizabilities tangential to the metasurface. In [20], the authors extended the work to include bianisotropic polarizabilities, in addition to those that are electric and magnetic. They provided closed-form expressions that relate the constituent sheet parameters to scattering parameters. The 4x4 scattering matrix for normal incidence was sufficient to calculate the tangential surface polarizabilities. However, if the scatterers composing the metasurface have polarizabilities in the normal direction as well, this method is unable to characterize it. In [12], the authors theoretically investigated the possibility of having scatterers with polarizabilities normal to the metasurface. However, very few experimental characterizations of such metasurfaces have been attempted to date. For instance, in [21] authors do not extract susceptibilities from experimental data, but they do compare theoretical to experimental scattering parameters for slabs with normal polarizabilities.

In this paper, we provide a compact and intuitive derivation of the sheet boundary conditions that model a metasurface with polarizabilities in the normal direction. In addition, we develop appropriate closed-form expressions that allow extraction of sheet susceptibilities from the free-space measurements of scattering parameters, for several different angles of incidence. Actually, these expressions can be thought of as a generalization of well-known case of normal incidence [20, 22]. Finally, the proposed extraction procedure is verified through full-wave simulations and the experimental characterization of the polarizabilities of a recently introduced DB metasurface [16] in 10 GHz band.

2. THEORY

Let us consider two half-spaces (Regions 1 and 2), described with intrinsic impedances η_1 and η_2, respectively. The half-spaces are separated by an infinite planar metasurface S located at $z = 0$. We will assume the z-direction ($\hat{a}_z$) to be normal to the metasurface, (see Fig. 1).

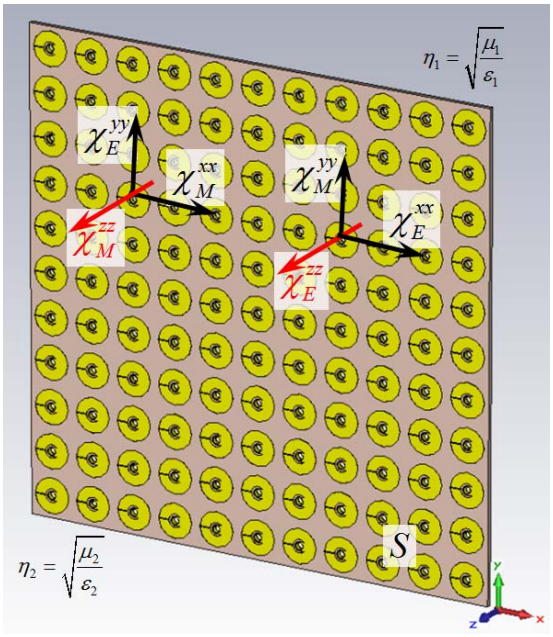

FIG. 1. Two-dimensional structure composed of periodically arranged scatterers, polarizable in all three spatial directions, is modeled as metasurface described with surface susceptibilities.

Also, the metasurface will be composed of periodically arranged scatterers, whose electric ($\vec{\vec{\chi}}_E$) and magnetic ($\vec{\vec{\chi}}_M$) susceptibilities can be described by diagonal tensors

$$\vec{\vec{\chi}}_E = \begin{bmatrix} \chi_E^{xx} & 0 & 0 \\ 0 & \chi_E^{yy} & 0 \\ 0 & 0 & \chi_E^{zz} \end{bmatrix}, \quad (1)$$

$$\vec{\vec{\chi}}_M = \begin{bmatrix} \chi_M^{xx} & 0 & 0 \\ 0 & \chi_M^{yy} & 0 \\ 0 & 0 & \chi_M^{zz} \end{bmatrix}. \quad (2)$$

Each tensor element has a unit of meter, and is related to the electric and magnetic polarizability densities of the scatterers per unit area, in its respective direction. The intent is to model such a physical metasurface with an impedance sheet boundary condition. This sheet boundary condition should relate electric and magnetic fields on both sides of the interface, taking into account the physical composition of the surface itself.

We begin by writing Faraday's and Ampere's laws. By separating all vectors into their transverse and longitudinal ($\hat{a}_z$) components, these two Maxwell's curl equations can be written as [23]

$$\begin{aligned} \nabla_t \times \vec{E}_t &= -\vec{M}_z - j\omega\mu\vec{H}_z \\ \nabla_t \times \vec{E}_z + \hat{a}_z \times \frac{\partial}{\partial z}\vec{E}_t &= -\vec{M}_t - j\omega\mu\vec{H}_t \end{aligned} \quad (3)$$

and

$$\begin{aligned} \nabla_t \times \vec{H}_t &= \vec{J}_z + j\omega\varepsilon\vec{E}_z \\ \nabla_t \times \vec{H}_z + \hat{a}_z \times \frac{\partial}{\partial z}\vec{H}_t &= \vec{J}_t + j\omega\varepsilon\vec{E}_t \end{aligned} \quad (4)$$

where $\vec{E}_t$ is transverse component of $\vec{E}$, $\vec{H}_t$ is transverse component of $\vec{H}$, $\vec{E}_z = E_z \cdot \hat{a}_z$, $\vec{H}_z = H_z \cdot \hat{a}_z$, $\nabla_t = \left(\frac{\partial}{\partial x}\hat{a}_x + \frac{\partial}{\partial y}\hat{a}_y\right)$. Applying (3) and (4) to a sheet at $z = 0$, that supports tangential and normal electric surface currents ($\vec{J} = \left(\vec{J}_{st} + \vec{J}_{sz}\right)\delta(z)$) and tangential and normal magnetic surface currents ($\vec{M} = \left(\vec{M}_{st} + \vec{M}_{sz}\right)\delta(z)$) yields the following expressions for the tangential field discontinuities at the sheet

$$\vec{E}\Big|_{z=0^-}^{0^+} \times \hat{a}_z = \vec{M}_{st} + \nabla_t\left(\frac{J_{sz}}{j\omega\varepsilon}\right) \times \hat{a}_z, \quad (5)$$

$$\hat{a}_z \times \vec{H}\Big|_{z=0^-}^{0^+} = \vec{J}_{st} - \hat{a}_z \times \nabla_t\left(\frac{M_{sz}}{j\mu\omega}\right). \quad (6)$$

If the magnetic surface currents are due to a surface magnetization (magnetic polarization) density $\vec{\mathsf{M}}_s$

$$\vec{M} = (\vec{M}_{st} + \vec{M}_{sz})\delta(z) = j\omega\mu\left(\vec{\mathsf{M}}_{st} + \vec{\mathsf{M}}_{sz}\right)\delta(z), \quad (7)$$

and the electric currents are due to an surface electric polarization density $\vec{\mathsf{P}}_s$

$$\vec{J} = (\vec{J}_{st} + \vec{J}_{sz})\delta(z) = j\omega\varepsilon\vec{\mathsf{P}}_s\delta(z) = j\omega\varepsilon\left(\vec{\mathsf{P}}_{st} + \vec{\mathsf{P}}_{sz}\right)\delta(z) \quad (8)$$

The tangential field discontinuities at the sheet ($z = 0$) can be rewritten as [23]

$$\vec{E}\Big|_{z=0^-}^{0^+} \times \hat{a}_z = j\omega\mu\vec{M}_{st} - \nabla_t\left(\frac{P_{sz}}{\varepsilon}\right) \times \hat{a}_z, \quad (9)$$

$$\hat{a}_z \times \vec{H}\Big|_{z=0^-}^{0^+} = j\omega\mu\vec{P}_{st} - \hat{a}_z \times \nabla_t M_{sz}. \quad (10)$$

Further, the surface magnetization density and surface electric polarization density can be expressed in terms of their respective polarizabilities in compact form as

$$\begin{aligned} \vec{P}_{st} &= \varepsilon \cdot \vec{\vec{\chi}}_E \cdot \vec{E}_t^{avg} \\ \vec{M}_{st} &= \mu \cdot \vec{\vec{\chi}}_M \cdot \vec{H}_t^{avg} \end{aligned} \quad (11)$$

for the tangential components, and

$$P_{sz} = \varepsilon \cdot \chi_E^{zz} \cdot E_z^{avg}$$
$$M_{sz} = \mu \cdot \chi_M^{zz} \cdot H_z^{avg} \quad (12)$$

for the normal components. Superscript *avg* denotes average field values at $z = 0$: $\vec{E}_t^{avg} = \left(\vec{E}_{t1} + \vec{E}_{t2}\right)/2$, $\vec{H}_t^{avg} = \left(\vec{H}_{t1} + \vec{H}_{t2}\right)/2$.

The outlined procedure results in the expressions that describe the transition of an electromagnetic wave trough a metasurface:

$$\hat{a}_z \times \left(\vec{E}_2 - \vec{E}_1\right) = -j\omega\mu\chi_M^{xx}\vec{H}_t^{avg} - \chi_E^{zz} \cdot \hat{a}_z \times \nabla_t \left(E_z^{avg}\right) \quad (13)$$

$$\hat{a}_z \times \left(\vec{H}_2 - \vec{H}_1\right) = j\omega\varepsilon\chi_E^{yy}\vec{E}_t^{avg} - \chi_M^{zz} \cdot \hat{a}_z \times \nabla_t \left(H_z^{avg}\right) \quad (14)$$

The electromagnetic properties arising from the physical arrangement of the scatterers are described by the surface susceptibility parameters χ. Equations of a similar form can be found in [12, 24] under the name "generalized sheet transition conditions", in [25, 26], or in terms of impedance boundary conditions in [27]. The left side of (13) and (14) represents the discontinuity in the tangential component of electric and magnetic field at the metasurface, respectively. The discontinuity of tangential electric field is proportional to magnetic sheet impedance Z_M, multiplied by averaged tangential magnetic field, yielding well-known impedance boundary condition

$$\vec{E}_t = \vec{\vec{Z}}_M \cdot \vec{H}_t, \quad (15)$$

where Z_M can be defined in terms of susceptibilities as

$$\vec{\vec{Z}}_M = -j\omega\mu\vec{\vec{\chi}}_M. \quad (16)$$

Another term that contributes to the electric field discontinuity at the surface is the scalar value of the normal component of electric field, averaged at $z = 0$ ($E_z^{avg} = \left(E_{z1} + E_{z2}\right)/2$). Due to duality, the gradient of this scalar function, vector-multiplied by normal unit vector, may be interpreted as tangential magnetic current that flows along the surface. Similar conclusions can be drawn for the discontinuity of tangential component of the magnetic field.

Let us now analyze the properties of a TE polarized plane wave obliquely incident (with angle θ) onto the previously described metasurface (see Fig. 2).

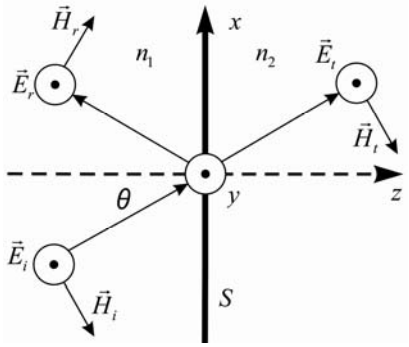

FIG. 2. TE polarized electromagnetic wave incident on metasurface *S* at arbitrary angle of incidence θ.

The components of the incident, reflected, and transmitted electric field can be expressed as

$$\vec{E}_i = \hat{a}_y \cdot E_0 \cdot e^{-j(\mathrm{x}k_0 \sin\theta + z k_0 \cos\theta)}$$
$$\vec{E}_r = \hat{a}_y \cdot S_{11}^{TE} \cdot E_0 \cdot e^{-j(\mathrm{x}k_0 \sin\theta - z k_0 \cos\theta)} \quad (17)$$
$$\vec{E}_t = \hat{a}_y \cdot S_{21}^{TE} \cdot E_0 \cdot e^{-j(\mathrm{x}k_0 \sin\theta + z k_0 \cos\theta)}$$

Similarly, the components of the incident, reflected, and transmitted magnetic field can be written as

$$\vec{H}_i = -\hat{a}_x \cdot \frac{E_0}{\eta_1}\cos\theta \cdot e^{-j(\mathrm{x}k_0 \sin\theta + z k_0 \cos\theta)} + \hat{a}_z \cdot \frac{E_0}{\eta_1}\sin\theta \cdot e^{-j(\mathrm{x}k_0 \sin\theta + z k_0 \cos\theta)}$$
$$\vec{H}_r = \hat{a}_x \cdot \frac{S_{11}^{TE}E_0}{\eta_1}\cos\theta \cdot e^{-j(\mathrm{x}k_0 \sin\theta - z k_0 \cos\theta)} + \hat{a}_z \cdot \frac{S_{11}^{TE}E_0}{\eta_1}\sin\theta \cdot e^{-j(\mathrm{x}k_0 \sin\theta - z k_0 \cos\theta)}$$
$$\vec{H}_t = -\hat{a}_x \cdot \frac{S_{21}^{TE}E_0}{\eta_2}\cos\theta \cdot e^{-j(\mathrm{x}k_0 \sin\theta + z k_0 \cos\theta)} + \hat{a}_z \cdot \frac{S_{21}^{TE}E_0}{\eta_2}\sin\theta \cdot e^{-j(\mathrm{x}k_0 \sin\theta + z k_0 \cos\theta)} \quad (18)$$

Since the $\boldsymbol{E}_z$ component is zero for TE polarization, expression (13) reduces to

$$\hat{a}_z \times \left(\vec{E}_2 - \vec{E}_1\right) = -j\omega\mu\chi_M^{xx}\vec{H}_t^{avg}. \quad (19)$$

Substituting (17) and (18) into (19), we can write expressions for the magnetic sheet susceptibility in transversal direction. First, the jump in tangential $\boldsymbol{E}$ field at $z = 0$ is found

$$\hat{a}_z \times \left(\vec{E}_2 - \vec{E}_1\right) = \hat{a}_x E_0 \cdot e^{-j(\mathrm{x}k_0 \sin\theta)}\left(S_{21}^{TE} - S_{11}^{TE} - 1\right). \quad (20)$$

Then, the average tangential $\boldsymbol{H}$ field at $z = 0$ is calculated

$$\vec{H}_t^{avg} = \hat{a}_x \cdot \frac{E_0}{2}\cos\theta \cdot e^{-j(\mathrm{x}k_0 \sin\theta)}\left(\frac{S_{11}^{TE}}{\eta_1} - \frac{S_{21}^{TE}}{\eta_2} - \frac{1}{\eta_1}\right) \quad (21)$$

Substituting (20) and (21) into (19) yields an expression for χ_M^{xx}

$$\chi_M^{xx} = \frac{2j}{\omega\mu_0\cos\theta}\frac{S_{21}^{TE} - S_{11}^{TE} - 1}{\frac{1}{\eta_1} + \frac{S_{21}^{TE}}{\eta_2} - \frac{S_{11}^{TE}}{\eta_1}}. \quad (22)$$

For $\eta_1 = \eta_2 = \eta_0$, (22) can be further reduced to

$$\chi_M^{xx} = \frac{2j\eta_0}{\omega\mu_0\cos\theta} \cdot \frac{S_{21}^{TE} - S_{11}^{TE} - 1}{S_{21}^{TE} - S_{11}^{TE} + 1}. \quad (23)$$

Furthermore, the electric susceptibility in the tangential direction (χ_E^{yy}) and the normal magnetic susceptibility (χ_M^{zz}), can be calculated from (14). Since (14) is one equation with two unknown surface parameters, two different sets of reflection and transmission measurements, at two arbitrary angles of incidence, are required. Since we can choose any arbitrary angle of incidence, it is most convenient to set one of them equal to 0° (i.e. normal incidence). In that case, the $\boldsymbol{H}_z$ component from (14) vanishes

$$\hat{a}_z \times \left(\vec{H}_2 - \vec{H}_1\right) = j\omega\mu\chi_E^{yy}\vec{E}_t^{avg}, \quad (24)$$

and χ_E^{yy} can be found by plugging expressions (17) and (18) into (24)

$$\chi_E^{yy} = \frac{2j}{\omega\varepsilon_0}\frac{\frac{S_{21}^{TE}}{\eta_2}+\frac{S_{11}^{TE}}{\eta_1}-\frac{1}{\eta_1}}{1+S_{11}^{TE}+S_{21}^{TE}}. \quad (25)$$

For $\eta_1 = \eta_2 = \eta_0$, (25) reduces to

$$\chi_E^{yy} = \frac{2j}{\omega\varepsilon_0\eta_0}\cdot\frac{S_{11}^{TE}+S_{21}^{TE}-1}{S_{11}^{TE}+S_{21}^{TE}+1}. \quad (26)$$

Therefore, one set of reflection and transmission parameters for normal incidence is required to calculate the sheet susceptibilities in the tangential directions. Comparing expressions (15) and (19), it can be deduced that the parameter χ_M^{xx} is related to magnetic sheet impedance

$$Z_M^{xx} = -j\omega\mu_0\mu_r\chi_M^{xx}. \quad (27)$$

Similarly, parameter χ_E^{yy} is related to the electric surface admittance

$$Y_E^{yy} = j\omega\varepsilon_0\varepsilon_r\chi_E^{yy}. \quad (28)$$

Once χ_E^{yy} is known, calculation of χ_M^{zz} is straightforward. In order to polarize magnetic scatterers in the direction normal to the metasurface, the incident electromagnetic wave must have a magnetic field component perpendicular to the surface. This is possible only for oblique incidence. The gradient of the averaged normal component of the H field yields a variation only in the x-direction

$$\chi_M^{zz}\cdot grad\left(H_z^{avg}\right) = \hat{a}_x\cdot\chi_M^{zz}\frac{\partial H_z^{avg}}{\partial x} \quad (29)$$

$$\hat{a}_z\times\chi_M^{zz}\cdot grad\left(H_z^{avg}\right) = -\hat{a}_y\chi_M^{zz}\,j\,\mathrm{k}_0\frac{E_0}{2}\sin^2\theta\cdot\ldots \\ \ldots\cdot\left(\frac{1}{\eta_1}+\frac{S_{11}^{TE}}{\eta_1}+\frac{S_{21}^{TE}}{\eta_2}\right)\cdot e^{-j(\mathrm{xk}_0\sin\theta)} \quad (30)$$

In these expressions, k_0 is the free-space wavenumber, while $S_{11}^{TE}(\theta)$ and $S_{21}^{TE}(\theta)$ are, respectively, reflection and transmission parameters obtained for an arbitrary angle of incidence $\theta \neq 0°$. In the analysis, it has been assumed that the sheet susceptibilities are independent of the angle of incidence. This statement will be confirmed by measurements in section 4. The expression for χ_M^{zz}, if $\eta_1 = \eta_2 = \eta_0$, is given below.

Next, we'd like to solve the forward problem. That is, we would like to predict the reflection and transmission properties of a given metasurface, provided that surface susceptibilities are known. We start with expression (23), which can be written in reduced form as

$$S_{11} = S_{21} - \frac{1+A}{1-A}, \quad (31)$$

where A is

$$A = \chi_M^{xx}\frac{\omega\mu_0\cos\theta}{2j\eta_0}. \quad (32)$$

Similarly, we can rewrite (35) as

$$S_{11} = -S_{21} + \frac{1-B}{1+B}, \quad (33)$$

where B is

$$B = \frac{-\chi_E^{yy}\eta_0\omega\varepsilon_0 - \chi_M^{zz}k_0\sin^2\theta}{2j\cos\theta}. \quad (34)$$

Solving the system of equations (31) and (33) yields expressions for the reflection (36) and transmission parameters (37).

Finally, it is convenient to express the magnetic surface susceptibility in the normal direction in terms of the other two sheet parameters, and measured transmission parameter. This is expression (38) obtained by performing an inversion on expression (37). It relates sheet parameters in the tangential direction (known from the normal incidence simulation or measurement) and simulated or measured S_{21} for oblique incidence, to the unknown magnetic surface susceptibility in the normal direction. This equation will prove essential for the calculation of normal magnetic sheet susceptibilities from the measurements.

$$\chi_M^{zz} = -\chi_E^{yy}\frac{\eta_0\omega\varepsilon_0}{\mathrm{k}_0\sin^2\theta} - \frac{2j\cos\theta}{\mathrm{k}_0\sin^2\theta}\cdot\frac{1-S_{11}^{TE}(\theta)-S_{21}^{TE}(\theta)}{1+S_{11}^{TE}(\theta)+S_{21}^{TE}(\theta)} \quad (35)$$

$$S_{11}^{TE}(\theta) = \frac{\frac{jk_0}{2\cos\theta}\left(\chi_M^{xx}\cos^2\theta - \chi_E^{yy} - \chi_M^{zz}\sin^2\theta\right)}{1-\frac{k_0^2}{4}\chi_M^{xx}\left(\chi_E^{yy}+\chi_M^{zz}\sin^2\theta\right)+\frac{jk_0}{2\cos\theta}\left(\chi_M^{xx}\cos^2\theta+\chi_E^{yy}+\chi_M^{zz}\sin^2\theta\right)} \quad (36)$$

$$S_{21}^{TE}(\theta) = \frac{1+\frac{k_0^2}{4}\chi_M^{xx}\left(\chi_E^{yy}+\chi_M^{zz}\sin^2\theta\right)}{1-\frac{k_0^2}{4}\chi_M^{xx}\left(\chi_E^{yy}+\chi_M^{zz}\sin^2\theta\right)+\frac{jk_0}{2\cos\theta}\left(\chi_M^{xx}\cos^2\theta+\chi_E^{yy}+\chi_M^{zz}\sin^2\theta\right)} \quad (37)$$

$$\chi_M^{zz} = \frac{\frac{-k_0^2}{4}\chi_M^{xx}\chi_E^{yy}\left[S_{21}^{TE}(\theta)+1\right]+S_{21}^{TE}(\theta)-1+\frac{jk_0 S_{21}^{TE}(\theta)}{2\cos\theta}\sin^2\theta}{\frac{k_0^2}{4}\chi_M^{xx}\sin^2\theta\cdot\left[S_{21}^{TE}(\theta)+1\right]-\frac{jk_0 S_{21}^{TE}(\theta)}{2\cos\theta}\sin^2\theta} \quad (38)$$

3. Numerical Parameter Extraction

We numerically tested a metasurface that exhibits both magnetic and electric polarizabilities in the normal direction. A good candidate for such a metasurface is a DB boundary metasurface. This metasurface was theoretically proposed in [28], while its first practical realization was reported in [16]. In brief, it is a metasurface that cancels the normal components of the ***D*** and ***B*** fields at a specified frequency of operation. This cancellation occurs due to polarization of the DB unit cell in the normal direction by both electric and magnetic fields. Since the free-space measurement system available to the authors was designed to operate in the X-band, the physical dimensions of the DB unit cell reported in [16] were redesigned to operate in this frequency band. A unit cell that achieves DB properties at 9.7 GHz is illustrated in Fig. 3.

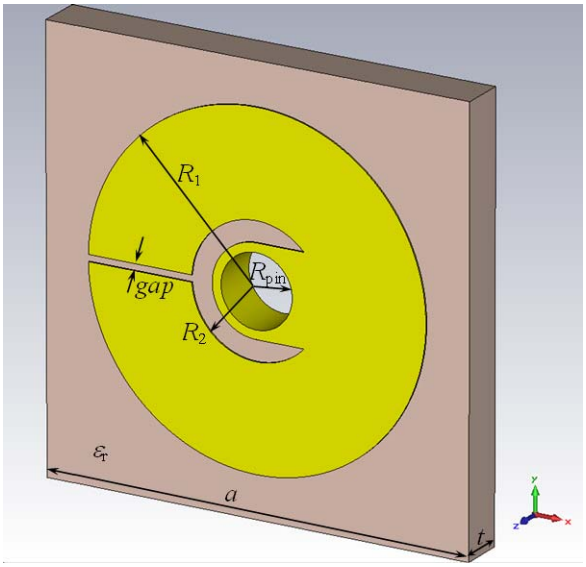

FIG. 3. DB unit cell designed to operate at 9.7 GHz. R_1 = 1.9 mm, R_2 = 0.73 mm, R_{pin} = 0.4 mm, gap = 0.075 mm, ε_r = 3.55 (RO4003C substrate), t = 0.508 mm, a = 4.75 mm.

Once designed, a series of scattering simulations were performed on the unit cell. The simulations were performed using frequency domain solver of the commercial electromagnetic software CST Microwave Studio™. The simulation setup is shown in Fig. 4. The unit cell was placed at z = 0, between two regions of space (η_1 and η_2). Since the metasurface was to be characterized in free space the wave impedances were set equal to that of vacuum: $\eta_1 = \eta_2 = \eta_0$. Infinite periodicity in the tangential directions (i.e. in the xy-plane) was enforced with periodic boundary conditions. Both the transmitting Floquet port 1 and the receiving Floquet port 2 were de-embedded to the front and the back face of the unit cell, respectively. Port 1 was excited by either normally or obliquely incident TE polarized plane waves. Scattering parameters S_{11} and S_{21} obtained from normal incidence simulations were used in (23) and (26) to calculate sheet susceptibilities in the tangential directions.

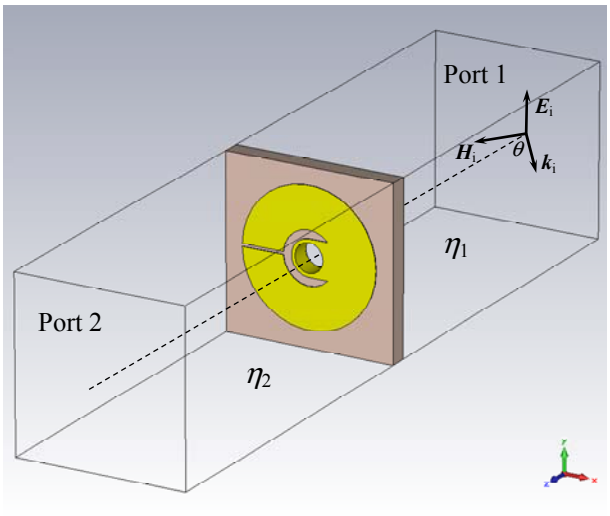

FIG. 4. Simulation setup used to retrieve surface parameters numerically. Floquet port 1 excites TE polarized plane waves at the arbitrary angle of incidence θ.

For oblique angles of incidence, the Floquet port modes ensured that the reflected wave was recorded in the direction of optical reflection, while the transmission was in the same direction as the incident wave. In this way it was possible to calculate the magnetic sheet susceptibility in the normal direction by using equation (35).

All the simulation results are presented in the next section and compared with free-space measurements on a fabricated sample.

4. Experimental Parameter Extraction

A DB metasurface consisting of the unit cells shown in Fig. 3, was fabricated using a commercial printed circuit board (PCB) fabrication process. A Rogers RO4003C substrate (ε_r = 3.55, tanδ = 0.0027, substrate thickness t = 0.508 mm) was used with a copper cladding thickness of 17 µm. The DB metasurface was 47 unit cells in the horizontal direction and 47 unit cells in the vertical direction, resulting in a physical dimension of 21 cm x 21 cm ($7\lambda_0$ x $7\lambda_0$, with λ_0 being the free-space wavelength). The fabricated metasurface is shown in Fig. 5 (a).

The DB metasurface was measured using the free-space X-band measurement setup illustrated in Fig. 5 (b) [29]. The setup is based on two quasi-optical Gaussian beam telescopes. Each telescope consisted of a vertically polarized rectangular horn antenna, with 25 dBi gain, and a pair of lenses separated for d = 90 cm. The lenses were identical, bi-hyperbolic in shape, and made of Rexolite (n = 1.59). The diameter of each lens was 32.5 cm with a focal distance of 45 cm. The transmitting horn antenna was connected to port 1 of a vector network analyzer (VNA) Agilent E8361A, while the receiving antenna was

connected to the port 2. The DB metasurface was fixed on a sample holder, 45 cm away from the telescopes.

The telescope was designed to produce a beam with 88% of its power coupled to the fundamental Gaussian mode. The pair of lenses focused this Gaussian beam to a beam whose size and location are independent of frequency [30, 31]. In [20], the focused Gaussian beam was measured and found to have a 114 mm beam waist diameter located 1.8 m from the phase center of the horn antenna. It was also found that the field measured at twice the beam waist (228 mm) was at least 25 dB below the peak value. Therefore, in order to avoid diffraction effects [30], the physical dimension of the fabricated DB metasurface was chosen to be twice the measured beam waist of the incident Gaussian beam.

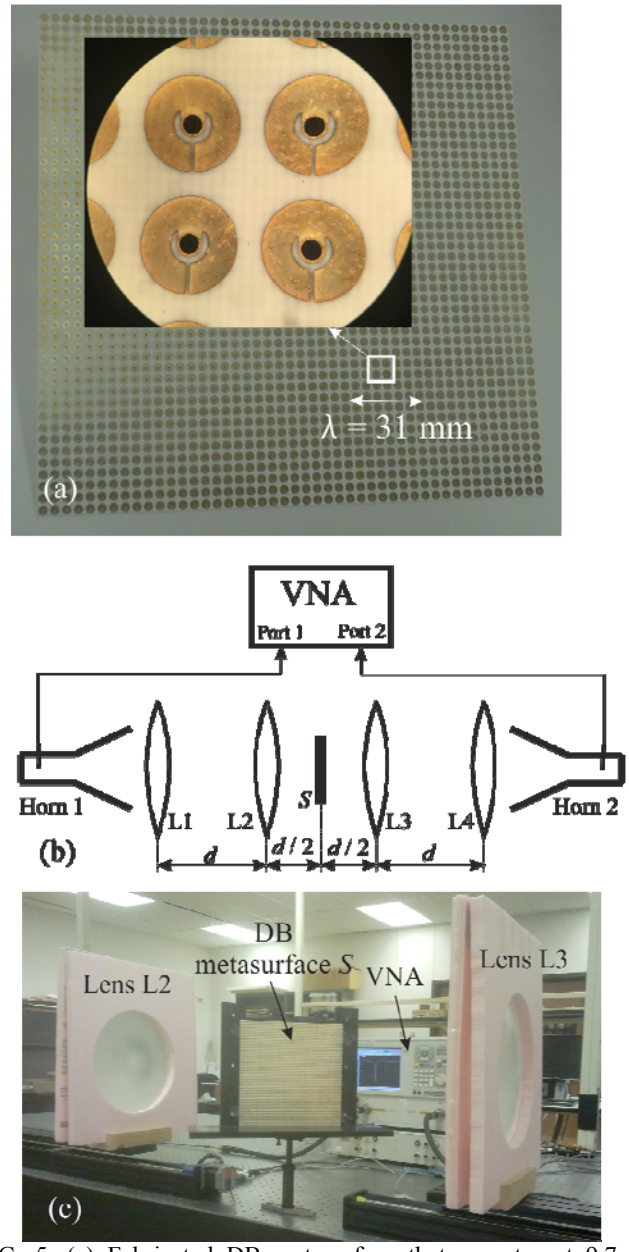

FIG. 5. (a) Fabricated DB metasurface that operates at 9.7 GHz, with enlarged segment detail. (b) Sketch of measurement setup formed of two X-band telescopes and VNA. (c) DB metasurface fixed on a sample holder during the oblique incidence measurement.

The free-space measurement setup was calibrated using the TRL (thru-reflect-line) method [32]. The reference planes for port 1 and port 2 were located at the focal planes of the transmitting and the receiving telescopes, respectively. A thru standard was configured by keeping the distance between the telescopes equal to twice the focal distance: 90 cm. The reflect standards for port 1 and port 2 were attained by placing a metal plate at the focal planes of the transmitting and the receiving telescopes, respectively. The reference planes corresponding to the transmitting and the receiving telescopes were located at the front and back faces of the metal plate, respectively. As result, the receiving reflector had to be moved back to account for the thickness of the metal plate. The line standard was achieved by separating the focal planes of the telescopes by a distance equal to a quarter of the free-space wavelength at the center of the band (i.e. at 10 GHz). Translation stages, with an accuracy of 5μm, were used to accurately move the telescopes. In the first step, the accuracy of the calibration procedure was assessed. For this purpose, the complex reflection coefficient of the metal plate and complex transmission coefficient of the thru setup were measured. A small ripple was observed in the measured S-parameters, which was caused by two factors. One cause of this irregularity was a small change in reference planes between calibration and measurement. This resulted from small changes in the position of the sample holder. One had to be careful to ensure good mechanical rigidity of the plates holding the sample, and avoid tilting of the sample. The second source of error was the presence of multiple reflections between the metasurface, lenses, and antennas. In order to remove the observed ripples, a standard time-gating technique was applied. It was found that the magnitude and the phase error in the measured reflection parameter of the metal plate was less than ±0.90 dB and ±0.6°, respectively. For the transmission parameter of the thru, the amplitude and the phase error were less than ±0.74 dB and ±0.8°, respectively.

After the calibration procedure was completed and verified, the DB metasurface was attached to the sample holder (Fig. 5(c)). The transmitting antenna illuminated the metasurface with a vertically-polarized TE wave. The transmitted TE wave was captured by the vertically-polarized, receive horn antenna. In the first set of measurements, scattering parameters (S_{11} and S_{21}) of the DB metasurface were measured for normal incidence. The measured complex scattering parameters are compared to those from simulation in Fig. 6.

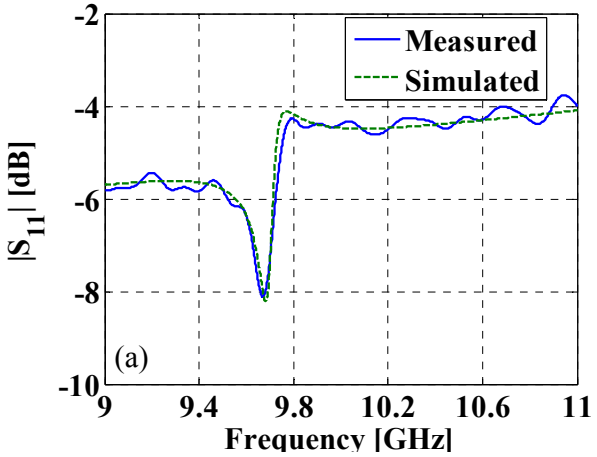

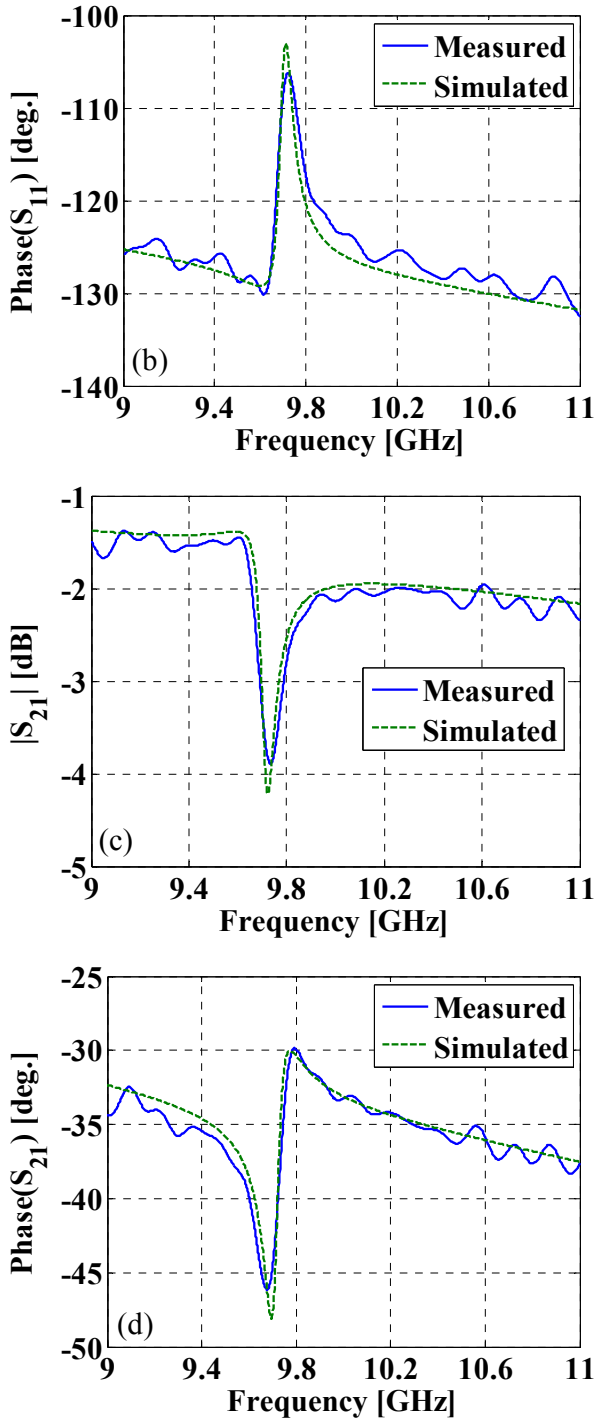

FIG. 6. Comparison between measured (solid) and simulated (dashed) scattering parameters of DB metasurface, for normal incidence. (a) Magnitude of the reflection parameter. (b) Phase of the reflection parameter. (c) Magnitude of the transmission parameter. (d) Phase of the transmission parameter.

It can be seen that the measured reflection and transmission parameters closely agree with those obtained from simulation. The small discrepancies can be attributed to slight misalignment of the measured metasurface from the focus of the Gaussian beam telescopes. The slight disagreement in "curve width" and ripples in the measured curves, outside the resonance region, are due to the inherent limitations of using time-gating with resonant structures [33].

The scattering parameters obtained from normal incidence measurements were substituted into expression (23) to extract the tangential magnetic sheet susceptibility. The obtained values for the real and imaginary parts are compared to those from simulation in Fig. 7.

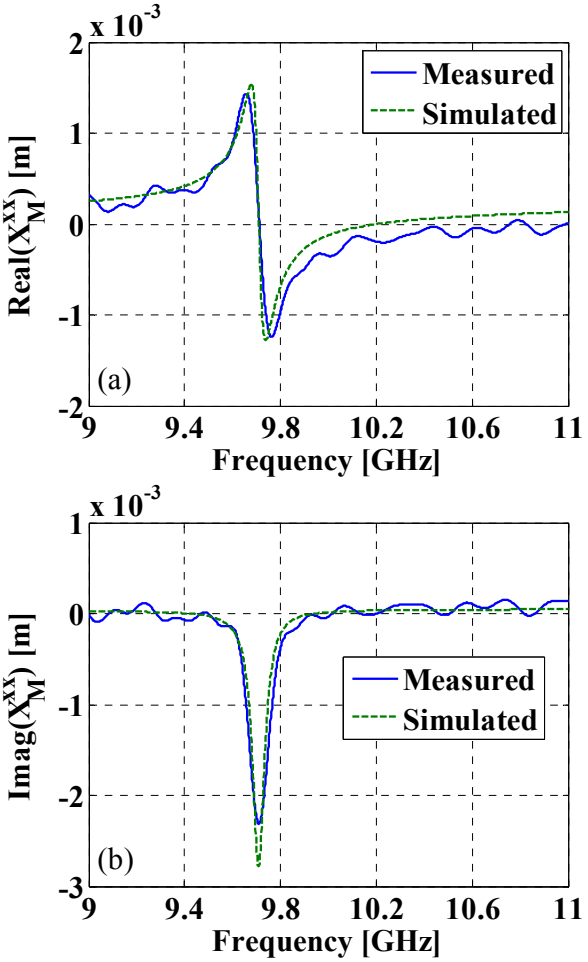

FIG. 7. Comparison between measured (solid) and simulated (dashed) magnetic surface susceptibility in the tangential direction χ_M^{xx}. (a) Real part. (b) Imaginary part.

The measured scattering parameters were also substituted into expression (26) to calculate the tangential electric sheet susceptibility. The obtained values for the real and imaginary parts are compared to those from simulation in Fig. 8.

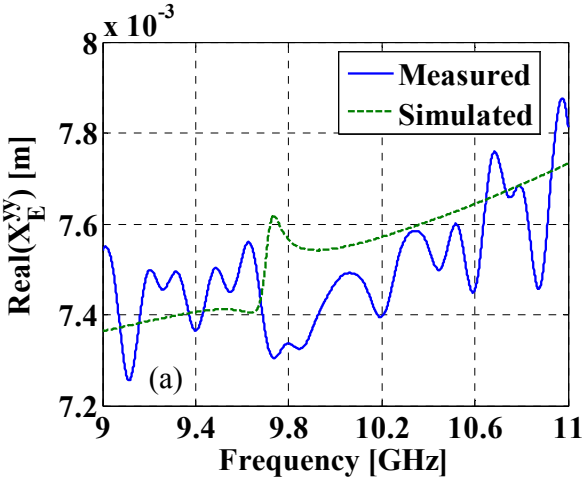

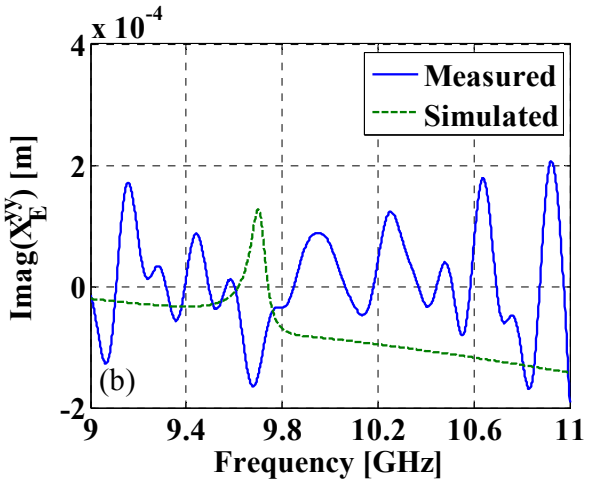

FIG. 8. Comparison between measured (solid) and simulated (dashed) electric surface susceptibility in the tangential direction χ_E^{yy}. (a) Real part. (b) Imaginary part.

After the sheet parameters in the tangential direction were retrieved from normal-incidence, the fabricated metasurface was excited with obliquely incident TE polarized waves. It was possible to accurately measure the fabricated metasurface for angles of incidence up to 60° from normal For angles of incidence beyond 60°, the metasurface would need to be much larger in order to avoid diffraction effects.

From the simulated sheet parameters, the complex transmission parameter was predicted as a function of angle of incidence at different frequencies using equation (37). The complex transmission parameter obtained in this way was then compared to the complex transmission parameter obtained from measurements of the fabricated DB metasurface. The comparison between the measured and predicted transmission parameter, for a 30° angle of incidence is shown in Fig. 9.

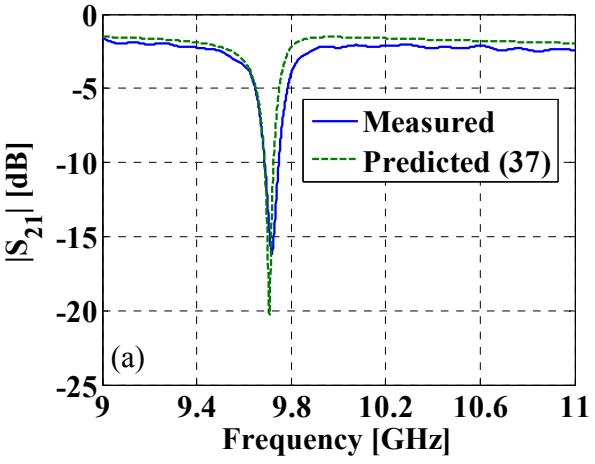

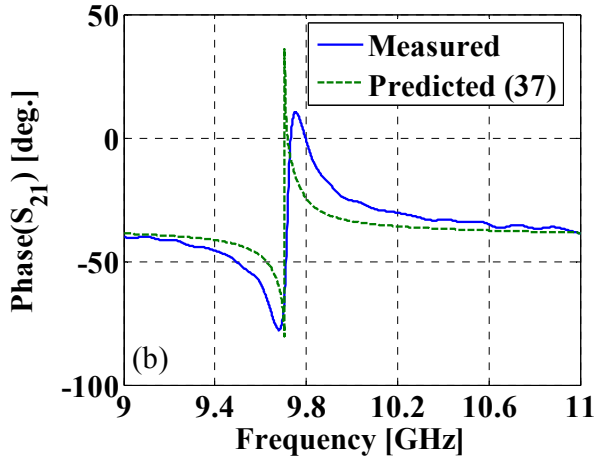

FIG. 9. Comparison between measured (solid) and theoretically predicted from eq. (37) (dashed) transmission parameter for angle of incidence $\theta = 30°$. (a) Magnitude. (b) Phase.

Finally, the magnetic sheet susceptibility in the normal direction was retrieved from the transmission measurements for three oblique angles of incidence (Fig. 10). For oblique angles of incidence, the reflected wave could not be measured using the experimental setup described, and equation (38) was employed.

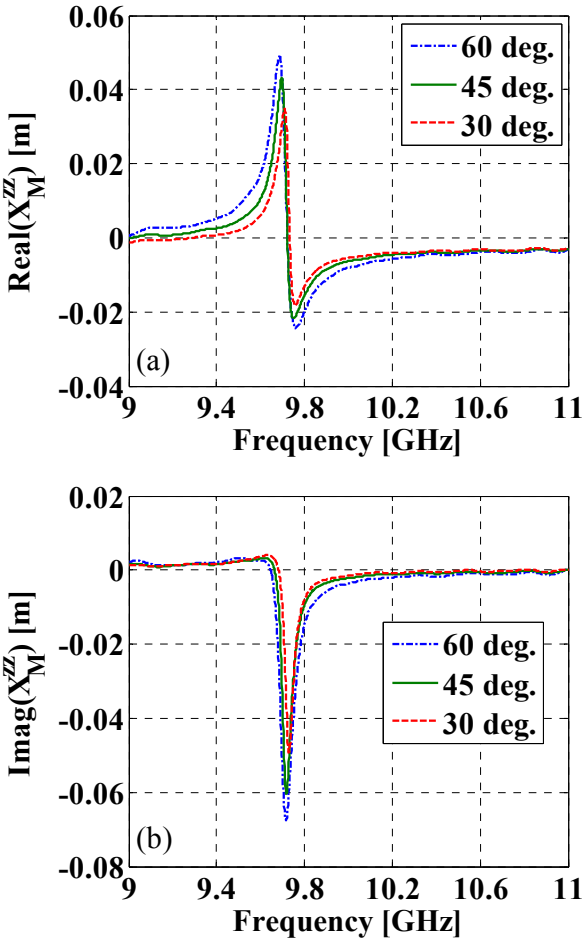

FIG. 10. Magnetic surface susceptibility in the normal direction χ_M^{zz} extracted from measurements and eq. (38) for several angles of incidence. (a) Real part. (b) Imaginary part.

5. CONCLUSIONS

In this paper, we provide full analytical, numerical, and experimental characterization of a metasurface with susceptibilities in all three spatial directions. A set of equations is derived that allows the physical surface distribution of scatterers to be replaced by a boundary condition, applied across an infinitely thin equivalent sheet. It is shown that an extraction of the unknown susceptibilities in the normal direction necessarily requires scattering parameters obtained from oblique incidence. Closed-form expressions that relate scattering parameters to surface susceptibilities in all three spatial directions are given. Reflection and transmission properties of the surface are predicted for an arbitrary angle of incidence, provided that constituent surface parameters are known. We also report the first full experimental characterization of a metasurface with polarizabilities in the normal direction. The free-space characterization was performed using a TRL calibration at 9.7 GHz on a recently proposed DB surface. Since the experimental set up did not allow the measurement of reflection parameters for oblique incidence, the sheet susceptibilities in the normal direction were extracted from measured transmission parameters alone. The sheet susceptibilities were shown not to change with angle of incidence, and therefore uniquely define the DB metasurface.

REFERENCES

[1] V. G. Veselago, "The Electrodynamics of Substances with Simultaneously Negative Values of ε and μ", Usp. Fiz. Nauk, 92, pp. 517-526, 1967.

[2] D. R. Smith, W. J. Padilla, D. C. Vier, S. C. Nemat-Nasser, and S. Schultz, "Composite Medium with Simultaneously Negative Permeability and Permittivity", Phys. Rev. Lett., 84, pp. 4184-4186, 2000.

[3] A. Grbic, and G. V. Eleftheriades, "Experimental verification of backward-wave radiation from a negative refractive index metamaterial", Journal of Applied Physics 92 (10), pp. 5930-5935, 2002.

[4] S. Hrabar, and J. Bartolić, "Experimental Investigation of Backward Meta-materials in Waveguide Environment", Proceedings on International Conference on Electromagnetics in Applied Applications, pp. 451 – 454, 2003.

[5] A. Grbic, and G. V. Eleftheriades, "Overcoming the diffraction limit with a planar left-handed transmission-line lens", Physical Review Letters 92 (11), 117403, 2004.

[6] S. Hrabar, Z. Šipuš, and J. Bartolić, "Experimental Verification of Negative Index of refraction by Lateral Beam Displacement", Proceedings of 2004 URSI EMTS Symposium, pp. 373 – 375, 2004.

[7] N. Engheta, and R. W. Ziolkowski, *Electromagnetic Metamaterials: Physics and Engineering Explorations*, John Wiley & Sons, Hoboken, NJ, 2006.

[8] G. V. Eleftheriades, and K. G. Balmain, *Negative Refraction Metamaterials: Fundamental Principles and Applications*, John Wiley & Sons, Hoboken, NJ, 2005.

[9] G. Bouchitté, and B. Schweizer, "Homogenization of Maxwell's Equations in a Split Ring Geometry", Multiscale Modeling Simulation, 8, 3, pp. 717-750, 2010.

[10] O. Acher, J.-M. Lerat, and N. Mallejac, "Evaluation and illustration of the properties of metamaterials using field summation", Optics Express 15, pp. 1096, 2007.

[11] S. Hrabar, and D. Zaluški, "Subwavelength Guiding of Electromagnetic Energy in Waveguide Filled with Anisotropic Mu-Negative Metamaterial", Electromagnetics, Vol 28, Is. 7, pp. 494 – 512, 2008.

[12] C. L. Holloway, E. F. Kuester, F. Edward, J. A. Gordon, and J. O'Hara, "An Overview of the Theory and Applications of Metasurfaces: The Two-Dimensional Equivalents of Metamaterials", IEEE Antennas and Propagation Magazine, Vol. 54, Is. 2, pp. 10 – 35, 2012.

[13] C. M. Roberts, S. Inampudi, and V. A. Podolskiy, "Diffractive interface theory: nonlocal susceptibility approach to the optics of metasurfaces", Optics Express 23, 2764-2776, 2015.

[14] C. Pfeiffer, and A. Grbic, "Metamaterial huygens surfaces: Tailoring wave fronts with reflectionless sheets", Phys. Rev. Lett, 110, pp. 197401, 2013.

[15] T. Niemi, A. Karilainen, and S. Tretyakov, "Synthesis of polarization transformers", IEEE Trans. on Antenn. And Propag., 61, pp. 3102 – 3111, 2013.

[16] D. Zaluški, S. Hrabar, and D. Muha, "Practical Realization of DB metasurface", Applied Physics Letters, 104, pp. 234106-1-234106-5, 2014.

[17] D. R. Smith, D. Schurig, and J. J. Mock, "Characterization of a Planar Artificial Magnetic Metamaterial Surface", Phys. Review E, 74, art. 036604, 2006.

[18] C. L. Holloway, E. F. Kuester, and A. Dienstfrey, "Characterizing Metafilms: The Connection Between Surface Susceptibilities and Effective Material Properties", IEEE Antennas and Wireless Propagation Letters, 2011.

[19] C. L. Holloway, A. Dienstfrey, E. F. Kuester, J. F. O'Hara, A. K. Azad, and A. J. Taylor, "A Discussion on the Interpretation and Characterization of Metafilms/Metasurfaces: The Two-Dimensional Equivalent of Metamaterials", Metamaterials, Vol. 3, Is. 2, pp. 100-112., 2009.

[20] C. Pfeiffer, and A. Grbic, "Bianisotropic metasurfaces for optimal polarization control: Analysis and synthesis", Physical Review Applied, 2 (4), 044011, 2014.

[21] C. L. Holloway, P. Kabos, M. A. Mohamed, E. F. Kuester, J. A. Gordon, M. D. Janezic, and J. Baker-Jarvis, "Realisation of a controllable metafilm / metasurface composed of resonant magnetodielectric particles: measurements and theory", IET Microw. Antennas Propag., 2010, Vol. 4, Is. 8, pp. 1111–1122, 2010.

[22] C. Pfeiffer, and A. Grbic, "Bianisotropic Metasurfaces: Ultra-thin Surfaces for Complete Control of Electromagnetic Wavefronts", arXiv preprint arXiv:1404.3313, 2014.

[23] J. A. Kong, *Electromagnetic Wave Theory*, Wiley-Interscience, 2008.

[24] E. F. Kuester, M. A. Mohamed, M. Piket-May, and C. L. Holloway, "Averaged Transition Conditions for Electromagnetic Fields at a Metafilm", IEEE Transactions on Antennas and Propagation, Vol. 51, No. 10, pp. 2641 – 2651, 2003.

[25] M. Idemen, and A. H. Serbest, "Boundary Conditions of the Electromagnetic Field", Electronics Letters, Vol. 23, No. 13, pp. 704 – 705, 1987.

[26] M. Idemen, "Straightforward Derivation of Boundary Conditions on Sheet Simulating an Anisotropic Thin Layer", Electronics Letters, Vol. 24, No. 11, pp. 663 – 665, 1988.

[27] T. B. A. Senior, and J. L. Volakis, *Approximate Boundary Conditions in Electromagnetics*, IET, 1995.

[28] I. V. Lindell, and A. Sihvola, "Electromagnetic DB boundary", Proceedings of the URSI Finnish XXXI Convention on Radio Science and Electromagnetics, pp. 81 – 82, 2008.

[29] S. M. Rudolph, C. Pfeiffer, and A. Grbic, "Design and Free-Space Measurements of Broadband, Low-Loss Negative-Permeability and Negative-Index Media", IEEE Antennas and Propagation, Vol. 59, Is. 8, pp. 2989 – 2997, 2011.

[30] P. F. Goldsmith, *Quasioptical Systems: Gaussian Beam Quasioptical Propogation and Applications*, Wiley-IEEE Pres, 1997.

[31] P. F. Goldsmith, "Quasi-optical Techniques", Proceedings of the IEEE, 80, pp. 1729 – 1747, 1992.

[32] D. K. Ghodgaonkar, V. V. Varadan, and V. K. Varadan, "A free-space method for measurement of dielectric constants and loss tangents at microwave frequencies", IEEE Trans. Instrum. Meas., vol. 38, pp. 789 – 793, 1989.

[33] M. Hiebel, *Fundamental of Vector network Analysis*, Rohde & Schwartz, Muenchen, Germany, 2007.